

Unstructured discretisation of a non-local transition model for turbomachinery flows

Andrea Ferrero^{*1}, Francesco Larocca^{2a} and Verena Bernaschek^{3b}

¹*INRIA Bordeaux Sud-Ouest and Université de Bordeaux, Talence, France*

²*Politecnico di Torino, Torino, Italy*

³*Technische Universität Braunschweig, Braunschweig, Germany*

(Received November 23, 2017, Revised January 5, 2017, Accepted January 6, 2017)

Abstract. The description of transitional flows by means of RANS equations is sometimes based on non-local approaches which require the computation of some boundary layer properties. In this work a non-local Laminar Kinetic Energy model is used to predict transitional and separated flows. Usually the non-local term of this model is evaluated along the grid lines of a structured mesh. An alternative approach, which does not rely on grid lines, is introduced in the present work. This new approach allows the use of fully unstructured meshes. Furthermore, it reduces the grid-dependence of the predicted results. The approach is employed to study the transitional flows in the T106c turbine cascade and around a NACA0021 airfoil by means of a discontinuous Galerkin method. The local nature of the discontinuous Galerkin reconstruction is exploited to implement an adaptive algorithm which automatically refines the mesh in the most significant regions.

Keywords: transition; laminar kinetic energy; unstructured mesh; discontinuous galerkin; adaptive mesh

1. Introduction

The study of transitional flows is one of the current challenges in computational fluid dynamics. Several efforts have been made in this field because the effects of transition can deeply influence the performances of industrial components. For instance, the optimization of low pressure gas turbines (LPT) is a key objective in the current design process of turbofan engines. The number of blades has been progressively reduced in order to minimize the total weight and to reduce the number of components. As a consequence, the blade loading has been increased by the development of high-lift and ultra-high lift blades. This trend has raised several aerodynamic issues which can influence the LPT's efficiency. For instance, the low Reynolds number which characterizes LPT blades at cruise conditions is usually associated to the presence of a laminar boundary layer on a large portion of the blade. This condition, together with the high turning angle of high-lift blades, can induce severe flow separations (Hourmouziadis 1989, Babajee 2013). The

*Corresponding author, Ph.D., E-mail: andrea.ferrero@inria.fr

^aProfessor, E-mail: francesco.larocca@polito.it

^bStudent, E-mail: v.bernaschek@tu-bs.de

extension of the separation region and the reattachment of the flow are significantly influenced by transition phenomena which can take place in the separation zone.

Similar problems can be encountered in the development of wind turbines. For example, some vertical axis wind turbines use symmetric airfoils which work with Reynolds numbers of the order of 10^5 . In these conditions, transition and separation phenomena can dramatically influence the performances. Furthermore, the increasing interest in Unmanned Aerial Vehicles (UAVs) has put in evidence several aerodynamics issues (Deters *et al.* 2014) related to low Reynolds number flows in which transition plays a fundamental role.

These motivations have promoted the development of numerical tools which can be used to predict both bypass and separation induced transition at relatively low Reynolds numbers. A review of the most common approaches was done by Tucker (2013).

Recently, Large Eddy Simulations (LES) and Direct Numerical Simulations (DNS) have been used to predict the behavior of low Reynolds number transitional flows in turbomachinery (Michelassi *et al.* 2002, De Wiart *et al.* 2012, De Wiart and Hillewaert 2015). These approaches reduce the need for problem-dependent turbulence closures by directly resolving turbulent structures. However, their computational cost becomes prohibitive when the Reynolds number is increased or when full annulus multistage configurations are considered.

In contrast, Reynolds Averaged Navier-Stokes (RANS) models are significantly cheaper but have some drawbacks in the modeling of transition. A simple algebraic transition model was proposed by Sjolander and Langtry (2002) for attached and separate flows. The same model was tested by Yershov and Yakovlev (2016) for the 3D flow in a turbine cascade showing an accuracy similar to several more complex models but with a significantly lower computational cost.

Some widely used transition models for RANS equations are based on the intermittency concept and require the introduction of additional transport equations. Typically, a transport equation is used to describe an intermittency variable which acts as a weighting factor to control the intensity of the production term in the RANS model. This approach requires the introduction of empirical correlations which have to be calibrated on the particular flow which is under study. An important contribution in this field was proposed by Langtry and Menter (2009) who introduced the $\gamma-Re_{\theta t}$ model. Thanks to an additional transport equation for the transition onset momentum thickness Reynolds number the $\gamma-Re_{\theta t}$ model works only on local quantities. Babajee (2013) performed a detailed analysis on the use of the $SST+\gamma-Re_{\theta t}$ model for the transitional flow in the T106c turbine cascade which is also studied in this work. A recent study on correlation based transition models in turbomachinery was proposed by Marciniak *et al.* (2014).

Recently, several transition models based on an alternative idea have been developed. They rely on the laminar kinetic energy (LKE) concept which was initially proposed by Mayle and Schulz (1997). The aim of this approach is the modeling of the pretransitional rise of fluctuations in transitional boundary layers and their subsequent breakdown to turbulence. This idea has been exploited by Walters and Leylek (2005) and Lardeau *et al.* (2004) to develop a model for natural and bypass transition. Walters and Cokljat (2008) proposed a three-equation laminar kinetic energy model which requires the evaluation of only local quantities. The laminar kinetic energy concept has been used also by Pacciani *et al.* (2011) for the study of transitional flows in low pressure gas turbines by a non-local three-equation model. This model was tested also by Marciniak (2015) showing good agreements with the experimental results when low Reynolds number flows are considered.

The model described in Pacciani *et al.* (2011) is considered in this work. It is a three-equation model which is based on the low Re Wilcox (1998) $k-\omega$ model with an additional equation for the

laminar kinetic energy. The source term in the LKE equation depends on the vorticity thickness of the shear layer and so it is non-local. A possible way of dealing with the computation of this term is to adopt a structured mesh and to evaluate the requested quantities along grid lines. This classical approach, which is very efficient, introduces some issues in the definition of a grid independent solution.

In order to avoid these issues, an alternative approach to the computation of the vorticity thickness is proposed in this work. The new approach does not rely on grid lines but uses test lines which reduce the grid-dependence. Furthermore, it can be applied to fully unstructured meshes which can be useful for the description of complex geometries in the presence of control devices.

Another important issue which arises in these kind of problems is the numerical description of the shear layer in the separated flow. Indeed, it is common practice to check the mesh resolution at the wall by monitoring the dimensionless mesh size (y^+). This guarantees that the boundary layer is properly solved but it does not give any information on the resolution of the shear layer in the separation region, because the shear layer is usually far from the wall. However, a proper description of the shear layer is crucial because one of the typical transition modes is related to the Kelvin-Helmholtz instability which takes place in the shear layer. In order to solve this issue, the use of an automatic adaptive algorithm is suggested in the present work. This algorithm can automatically detect the regions in which the discretization error is larger and refine the mesh locally by splitting. The non-conforming mesh which is obtained after this process can be easily managed by the discontinuous Galerkin (DG) approach which was chosen to discretize the governing equations.

The proposed approach is applied to the prediction of the transitional flow in the T106c turbine cascade and the results are compared with the experimental data. In particular, the computations are carried out on several meshes (both structured and unstructured) in order to understand the grid dependency effects and show the benefits offered by the automatic adaptive algorithm.

Finally, the transitional separated flow over a NACA0021 airfoil is studied and compared with the experimental data and the results obtained by other models in both pre-stall and post-stall working conditions.

2. Physical model

In this work the 2D Reynolds Averaged Navier-Stokes equations are considered. Turbulence closure is performed by means of a three-equation model based on the laminar kinetic energy approach (Pacciani *et al.* 2011) which is reported in the following

$$\frac{\partial \rho k}{\partial t} + \frac{\partial(\rho u_j k)}{\partial x_j} = P - \beta^* \rho k \omega + \frac{\partial}{\partial x_j} \left[(\mu + \sigma_k \mu_t) \frac{\partial k}{\partial x_j} \right] + \rho R \quad (1)$$

$$\frac{\partial \rho \omega}{\partial t} + \frac{\partial(\rho u_j \omega)}{\partial x_j} = \frac{\alpha \omega P}{k} - \beta \rho \omega^2 + \frac{\partial}{\partial x_j} \left[(\mu + \sigma_\omega \mu_t) \frac{\partial \omega}{\partial x_j} \right] \quad (2)$$

$$\frac{\partial \rho k_L}{\partial t} + \frac{\partial(\rho u_j k_L)}{\partial x_j} - \frac{\partial}{\partial x_j} \left(\mu \frac{\partial k_L}{\partial x_j} \right) = \rho \nu_L S^2 - 2\mu \frac{k_L}{d^2} - \rho R \quad (3)$$

The first two equations of this model are derived from the original low Reynolds version of the

Wilcox (1998) k - ω model and all the constants and variables are defined according to that work. The third equation describes the evolution of the laminar kinetic energy. In the Eq. (1) there is an additional term (ρR) with respect to the original Wilcox (1998) k - ω model. This term represents the coupling between the turbulent kinetic energy field and the laminar kinetic energy field. Eq. (3) describes the evolution of the laminar kinetic energy k_L .

On the right hand side there are a production term, a destruction term and a coupling term, respectively. The coupling term appears with opposite sign also in the turbulent kinetic energy equation and is responsible for the activation of the transition.

The production term in the k_L equation depends on the ‘‘laminar eddy viscosity’’ ν_L

$$\nu_L = C_1 \sqrt{k_L} \delta_\Omega \quad (4)$$

The constant C_1 has to be deduced from calibration. In Pacciani *et al.* (2011) it is set to $C_1=0.01$. In the present work the value $C_1=0.0075$ is chosen.

The variable δ_Ω is the vorticity thickness. It is responsible for the non-local behavior of the model as will be explained in Section 5.

The transfer term R is computed as

$$R = C_2 f_2 \omega \beta^* k_L \quad (5)$$

The damping function f_2 is

$$f_2 = 1 - e^{-\frac{\psi}{C_3}} \quad \psi = \max(0, R_y - C_4) \quad (6)$$

The constant C_2 regulates the intensity of the energy transfer from k_L to k and is set to $C_2=0.3$, according to Pacciani *et al.* (2011).

The constant C_4 represents a threshold for the activation of transition and it is set to $C_4 = 10$, according to Pacciani *et al.* (2011). This threshold is compared with the variable $R_y = \sqrt{k}d/\nu$ which can be seen as a local Reynolds number based on the turbulent kinetic energy k and the wall distance d . Finally, the constant C_3 is set as $C_3=8$.

In the code all the equations are solved in non-dimensional form. After nondimensionalization, the ω equation is transformed by considering the logarithm of ω instead of ω itself.

This is done to improve the robustness of the discretization, following the guidelines of Bassi *et al.* (2005). Also the value of k and ω employed in the source terms of Eqs. (1) and (2) are evaluated following the realizability conditions suggested by Bassi *et al.* (2005).

2.1 Issues related to external flows

In the present work, the Eqs. (1), (2) and (3) are used for turbulence closure when studying internal flows in turbomachinery. However, the study of external flows requires particular care in the choice of boundary conditions. Indeed, the Eqs. (1) and (2) introduce an exponential decay of the turbulence variables between the inlet boundary and the leading edge. In turbomachinery flows this phenomenon is taken into account by choosing the proper value of ω_{in} which gives the best agreement between the computed turbulence decay and the experimental values (Bode *et al.* 2014). In external flows, a similar procedure can be used by setting an arbitrary large value of k_∞ and performing a trial and error study which allows to identify the proper value of ω_∞ required to get a turbulence level at the leading edge close to the chosen working condition. An example of this second approach is described by Choudhry *et al.* (2015) for the study of the flow around the

NACA0021 airfoil.

However, this methodology can introduce some difficulties when the solution of the problem is obtained by adaptive algorithms. Indeed, an adaptive simulation is usually started on a very coarse mesh which is usually not able to properly describe the turbulence decay between the inlet (which can be very far from the body in external flows) and the leading edge. In this way, it is difficult to get the chosen turbulence level at the leading edge and at each refinement step the airfoil will be subjected to a different incoming turbulence level. Furthermore, a wrong turbulence level close to the airfoil is even more problematic due to a particular feature of the chosen laminar kinetic energy model (Pacciani *et al.* 2011). In particular, the coupling term between laminar and turbulent kinetic energy is controlled by the damping function f_2 which depends on the turbulent kinetic energy and not on the laminar kinetic energy. For this reason, if the turbulence level of the flow which reaches the airfoil is too low then the transition could never start because the produced laminar kinetic energy is not transferred to the turbulent kinetic energy field.

In order to solve this issue, some sustaining terms are introduced in the present work, following the same approach proposed for the SST model by Spalart and Rumsey (2007). In particular, the following corrections \tilde{P}_k and \tilde{P}_ω are added to the right hand side of Eqs. (1) and (2), respectively.

$$\tilde{P}_k = \beta^* \rho_\infty k_\infty \omega_\infty \quad \tilde{P}_\omega = \beta \rho_\infty \omega_\infty^2 \quad (7)$$

These additional terms prevent the turbulence decay in the far field because they compensate the destruction terms here. However, their magnitude is negligible when compared to the original production and destruction terms close to the body. In the present work, the sustaining terms \tilde{P}_k and \tilde{P}_ω are proposed only for external flows.

They do not alter the transition phenomenon in the considered flow because the laminar kinetic energy produced in the shear layer and the related coupling term (which injects energy in the turbulent kinetic energy equation) are significantly larger than the far field turbulent kinetic energy. This can be verified by the turbulent kinetic energy field obtained in the test case of Section 7 and reported in Figs. 7 and 9. For other flows characterized by a large turbulence intensity in the far field, the use of the sustaining term can be questionable since they can become comparable to the original source terms of the model and so they can affect in a non-physical way the transition phenomena. However, in the present work they are used only for an external flow characterized by a very low level of free stream turbulence.

3. Numerical framework

The simulations are performed by an unstructured research code based on the discontinuous Galerkin (DG) approach. The numerical solution inside each element is described by an orthonormal basis obtained by the modified Gram-Schmidt orthonormalization algorithm, following the guidelines of Bassi *et al.* (2012). The orthonormalization algorithm is initialized by a monomial basis defined in the physical space. Second (DG1) and third order (DG2) accurate discontinuous Galerkin methods are chosen for this work. Wall elements have parabolic edges for DG1 and cubic edges for DG2. Convective fluxes are computed by means of an approximate Riemann problem solver (Osher and Solomon 1982, Pandolfi 1984). Diffusive fluxes are computed by means of a recovery-based approach (Ferrero *et al.* 2015).

As far as time integration is concerned, the backward Euler method is used. In order to

accelerate the convergence to the steady state solution a CFL evolution strategy is used following the approach of Bassi *et al.* (2010). The minimum CFL number is 1 and the maximum CFL number is 10^4 . The linear system resulting from the implicit discretization is solved by means of the restarted GMRES algorithm with ILU0 preconditioner. The PARALUTION library (Lukarski and Trost 2014) is used for this purpose. The stopping criteria for the GMRES iterative solver are based on a relative tolerance equal to 10^{-5} and a maximum number of iterations equal to 1000. The dimension of the Krylov subspace is 100. The meshes are generated by the free software package Gmsh (Geuzaine and Remacle 2009).

4. Adaptive algorithm

The adaptive algorithm used in this work is based on isotropic splitting of the elements which show the largest discretization errors. When an element needs to be refined it is switched off and substituted by four smaller elements. The resulting mesh can be non-conforming but this is easily managed because the reconstruction in the DG approach is local and involves only the degrees of freedom of the element.

Particular care is required when refining wall elements. Indeed, the DG approach requires curvilinear elements at wall to describe accurately the wall shape (parabolic elements in this work).

For this reason, when an element close to the wall is split it is necessary to use a parametric representation of the wall shape to generate the additional points required by the new curvilinear elements. In the present approach this is done by performing a spline interpolation of the original wall points.

The adaptive algorithm is driven by a sensor based on the residuals of the discretization, following the approach of Leicht and Hartmann (2010). This sensor gives an estimate of the discretization error for all the conservative equations inside each element. The evaluation of the error indicator in all the domain makes it possible to perform the refinement of the elements which show the largest errors. In particular, a fixed fraction ε of the total number of elements N is split.

When this procedure is applied on a system of conservative equations, the list of elements which should be refined can be obtained by putting together the lists obtained independently by the application of the previous procedure on each conservative equation. Since the error distribution is not identical for all the equations, the final refinement fraction will be larger than ε .

However, this approach guarantees that for each considered equation at least the worst εN elements are refined. For example, if the refinement fraction is set to $\varepsilon=10\%$ then the total number of elements is increased by a factor larger or equal to $(1-\varepsilon)+4\varepsilon=1.3$ at each call of the adaptive algorithm.

Since the chosen sensor refers to steady equations it is necessary to reach an approximately steady solution before performing a new adaptation. In this work, the adaptation is performed when the L2-norm of the non-dimensional x-momentum residual drops down 10^{-5} .

5. Vorticity thickness

The vorticity thickness is related to the thickness of the shear layer and so it gives an estimation

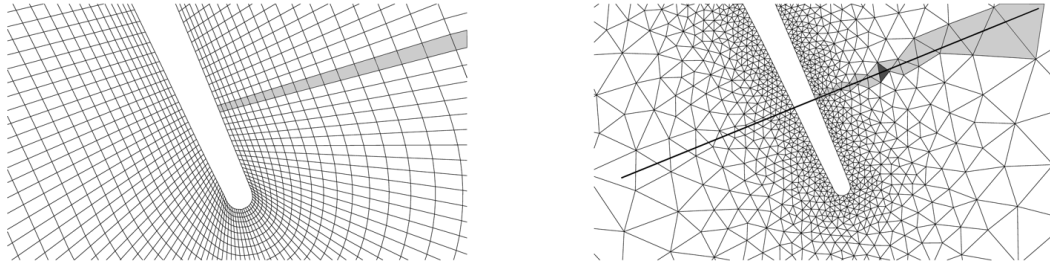


Fig. 1 Evaluation of vorticity thickness along grid lines (left) and test lines (right)

of the length scale of the structures which can appear in the transitional region. It can be evaluated by the following approximation (Pacciani *et al.* 2011)

$$\delta_{\Omega} = \frac{V_{\infty} - V_0}{2} \left(\frac{\partial V}{\partial y} \right)_{max_y}^{-1} \tag{8}$$

where V_{∞} is the “freestream” velocity magnitude, V_0 is the wall velocity magnitude (zero for fixed bodies) and $\frac{\partial V}{\partial y}$ is the derivative of the velocity magnitude with respect to the wall normal coordinate y . The value of V_{∞} can be estimated by the velocity value at the edge of the boundary layer.

In order to correctly evaluate the thickness of the shear layer both $\left(\frac{\partial V}{\partial y} \right)_{max_y}^{-1}$ and V_{∞} should be evaluated along “test lines” normal to the streamlines. On a flat plate, this can be done by considering the wall normal direction since the streamlines are approximately aligned to the wall. This is no more true when a general body is considered. For example, this approach fails to predict the thickness of the shear layer in the zone close to the trailing edge of an airfoil because in this region the wall normal lines are approximately aligned with the wake and so they are no more normal to the streamlines. A possible remedy for this issue is presented in Section 5.3.

When a proper “search line” has been defined, it is necessary to identify the edge of the boundary layer in order to evaluate V_{∞} . This can be done by looking for the maximum total pressure along the search line: the edge of the boundary layer can be approximated by the element closest to wall in which the total pressure is greater than 98% of the maximum total pressure along that line, according to Kozulovic and Lapworth (2007).

5.1 Evaluation of vorticity thickness along grid lines

The simplest way of computing the vorticity thickness is to evaluate Eq. (8) along the wall normal grid lines of a structured mesh. In Fig. 1 on the left an example of this procedure is reported. For each element of the gray row the same vorticity thickness is assigned. This approach implies that the domain of dependency of each element is completely defined by the direction of the grid lines. It is possible to define a structured mesh close to the wall surrounded by an unstructured mesh, provided that the structured region is sufficiently large to contain the shear layer. In the external unstructured region, the vorticity thickness can be set equal to zero.

The main problem of the grid lines approach is that it is not sufficient to perform a grid refinement study to obtain a grid independent solution. This is due to the fact that the source term

depends not only on the mesh size but also on the direction of the grid lines which influences the choice of the data used to evaluate the vorticity thickness.

5.2 Evaluation of vorticity thickness along test lines

In order to reduce the dependency of the solution on the direction of the grid lines an alternative approach based on “test lines” is introduced. Furthermore, this approach makes it possible to use fully unstructured discretizations which can be useful in the presence of complex geometries. For each element, a test line is defined as the line which passes through its center and is normal to the wall. In order to identify the direction of the test line it is possible to consider the vector between the center of the element and the closest wall point. Alternatively, the direction can be obtained by the gradient of the wall distance field which is known in all the internal quadrature points of the element because it is required by the source terms of the model.

In Fig. 1 on the right the concept is applied to a generic element in an unstructured mesh. The vorticity thickness in the considered element (the dark element in the picture) will be computed by taking the information from a list of elements which is found by considering the intersection between the test line and all the elements in the mesh. This test list must include only the elements which come from the side of the airfoil in which there is the considered element (see gray elements in Fig. 1 on the right). This selection can be done by computing the dot product between the wall distance gradients in the considered element and in the candidate element: only the elements for which the dot product is positive are inserted into the test list.

The described procedure can be applied as a preprocessing step at the beginning of the simulation and the list can be stored in the memory and used during the computations.

In order to reduce the computational cost and the memory requirements it is possible to define a threshold such that the procedure is avoided for the elements whose wall distance is greater than the threshold. In these far field elements, which are not involved in the transition process when the threshold is sufficiently large, the vorticity thickness can be set equal to zero. Furthermore, they can be neglected in the test lists of all the other elements.

A similar approach has been already introduced by Kozulovic and Lapworth (2007). However, their approach is based on test lines which are built by connecting the grid points and so it is equivalent to the grid lines approach. Such a procedure would be very complicated in the presence of unstructured triangular meshes because the obtained test lines would not be straight lines. In contrast, the approach proposed in this paper does not use the grid points and so the resulting test lines are always straight lines, independently from the mesh. For this reason, the presented approach can be considered a generalization of the procedure proposed by Kozulovic and Lapworth (2007).

5.3 Vorticity thickness correction

The definition of vorticity thickness given at the beginning of this Section can give unphysical results along the test lines which start from the leading edge and the trailing edge. This is due to the fact that these test lines are far from being perpendicular to the streamlines and so the corresponding vorticity thickness estimate can be very inaccurate. At a first glance, this problem could appear negligible because the transition process usually appears before the trailing edge and so the flow in the trailing edge region should be already turbulent. However, the unphysical vorticity thickness obtained in this region can introduce numerical problems related to the

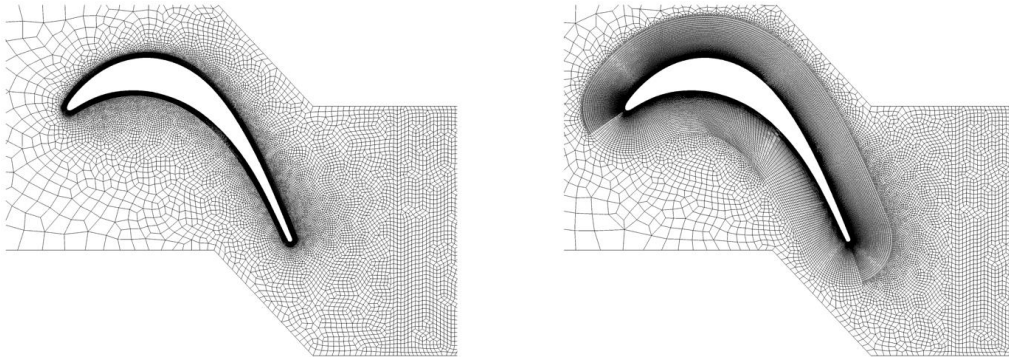


Fig. 2 Mesh A (left) and B (right): Thin and large structured region surrounded by an unstructured region

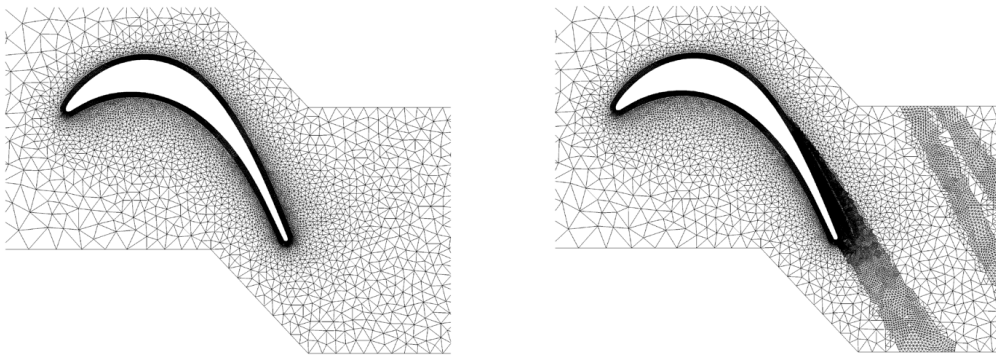


Fig. 3 Mesh C (left) and D (right): Original and adapted fully unstructured meshes

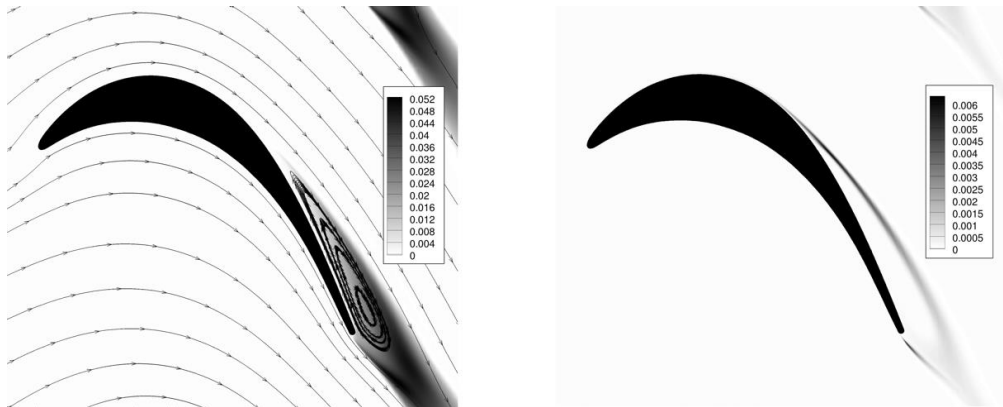


Fig. 4 T106c cascade: Dimensionless turbulent kinetic energy ($k/\mathcal{R}T_{in}^0$) with streamlines (left) and dimensionless laminar kinetic energy ($k_L/\mathcal{R}T_{in}^0$) (right)

integration of the governing equations. For this reason, a simple remedy is adopted in the present work. In particular, the vorticity thickness for all the elements whose center is behind $x_{LE}+0.99(x_{TE}-x_{LE})$ is set equal to the average of the vorticity thickness values which characterize the wall elements whose center is between $x_{LE}+0.95(x_{TE}-x_{LE})$ and $x_{LE}+0.99(x_{TE}-x_{LE})$. Here x_{LE} and x_{TE} represent the x coordinate of the leading and trailing edge, respectively.

Furthermore, the vorticity thickness for all the elements whose center is before the leading edge is set equal to zero. In this way, the correct vorticity thickness estimate is kept on the suction and pressure sides. At the same time, the unphysical values far from the blade are removed. Even if the imposed values in these regions are just a rough estimate they do not influence significantly the solution because usually the flow is already turbulent after the trailing edge and so the transition source terms are here negligible with respect to the turbulence source terms.

6. T106c turbine cascade at $M_{2s}=0.65$ and $Re_{2s}=80000$

The flow in the T106c turbine cascade has been experimentally investigated (Michalek *et al.* 2012) for several working conditions. Here a working condition characterized by an open separation is considered. In particular, the boundary layer separates where it is still laminar and then it fails to reattach. The transition to turbulence is localized in the separation region.

The isentropic exit Reynolds number is $Re_{2s}=8 \cdot 10^4$ and the isentropic exit Mach number is $M_{2s}=0.65$. The inlet angle is $\alpha_{in}=32.7^\circ$ and the inlet turbulence level is $Tu_{in}=0.8\%$. In the simulations the inlet laminar kinetic energy is set equal to the inlet turbulent kinetic energy according to Pacciani *et al.* (2011). The specific dissipation at the inlet is computed as $\omega_{in} = \sqrt{k_{in}/l_t}$ where the turbulence length scale (l_t) is set to $l_t=2.5 \cdot 10^{-3} c_x$ (where c_x is the axial chord) according to the turbulence decay study performed by Pacciani *et al.* (2011).

The simulations are carried out on four different meshes in order to test the behavior of the proposed approach. All simulations are performed by means of a second order accurate scheme. Mesh A is characterized by a thin structured region close to the wall surrounded by an unstructured grid of quadrilaterals (Fig. 2 on the left). It contains 46238 quadrilaterals.

Mesh B is similar to mesh A but the extension of the structured region is significantly larger (Fig. 2 on the right) and it contains 54375 quadrilaterals.

In contrast, mesh C is based on a fully unstructured discretization (Fig. 3 on the left) and contains 23796 triangles.

Starting from the solution on mesh C the adaptive algorithm is called twice and mesh D is obtained (Fig. 3 on the right). It can be seen that the algorithm is able to detect the recirculation bubble and the shear layers.

The meshes A, B, D are characterized by a dimensionless wall distance $y^+ < 1$ over all the wall, with the exception of some points close to the leading edge.

The turbulent kinetic energy (k) field and some streamlines are shown in Fig. 4, putting in evidence the structure of the recirculation bubble. The turbulence kinetic energy is normalized with respect to $\mathcal{R}T_{in}^0$ where \mathcal{R} is the specific gas constant and T_{in}^0 is the total temperature at inlet. The Fig. 4 shows also the laminar kinetic energy field (k_L) obtained on mesh D. This puts in evidence the position of the shear layers.

The wall isentropic Mach number distribution for the four meshes is reported in Fig. 5. The plot shows that the proposed approach can give results which are in reasonable agreement with the experimental data even when very different meshes are chosen. The plot shows also the results obtained by Babajee (2013) with the $\gamma-Re_{\theta t}$ transition model. In particular, Babajee (2013) performed a study on the influence of the inlet turbulence length scale. He showed that the turbulence length scale obtained by fitting the experimental turbulence decay of the wind tunnel does not give a good agreement on the T106c test case (see Fig. 5) when the $\gamma-Re_{\theta t}$ transition model is used. For this reason, he tried several different values of the turbulence length scale and

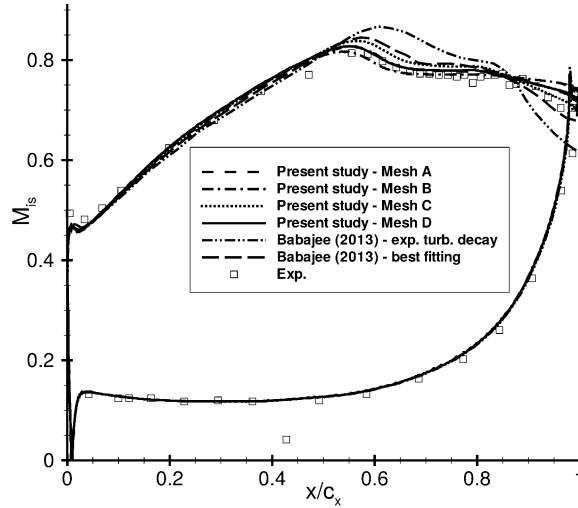


Fig. 5 T106c cascade: Wall isentropic Mach number distribution for different meshes

the best obtained results (related to a turbulence length scale which is several orders of magnitude different from the value obtained by fitting the tunnel’s turbulence decay) are reported in Fig. 5.

7. NACA0021 airfoil at $Re_\infty=120000$

In this Section the transitional flow around a NACA0021 airfoil is considered with reference to the experimental setup described by Hansen *et al.* (2011). The Reynolds number is relatively low ($Re_\infty=1.2 \cdot 10^5$) and this makes this test case representative for the blades of some vertical axis wind turbines or for the flows which characterize some Unmanned Aerial Vehicles. The freestream Mach number is set to $M_\infty=0.2$.

The far field is set at 20 chords from the airfoil according to the conditions chosen by Choudhry *et al.* (2015) for their numerical study on this test case. The far field turbulent kinetic energy level is set equal to the experimental value $Tu_\infty=0.6\%$. Thanks to the introduced sustaining terms this value is preserved up to the airfoil.

The specific dissipation rate in the far field is set to $\omega_\infty=5u_\infty/c_x$, following the recommendation of Spalart and Rumsey (2007) for the modified SST model with sustaining terms. Usually, the value of ω_∞ for the $k-\omega$ model in external flows is chosen by a trial and error procedure which is used to reproduce the decay of the turbulence level from an arbitrary large inlet value to the required leading edge value (Choudhry *et al.* 2015). Since here the turbulence decay in the freestream is removed this alternative approach cannot be used and so the previously described boundary condition is adopted.

In the following, two working conditions are considered in order to evaluate the behavior of the proposed approach in the presence of a small recirculation bubble and a large stall.

7.1 Pre-stall working condition: $\alpha_\infty=10^\circ$

The experimental data for an angle of attack $\alpha_\infty=10^\circ$ and a Reynolds number $Re_\infty=1.2 \cdot 10^5$ show

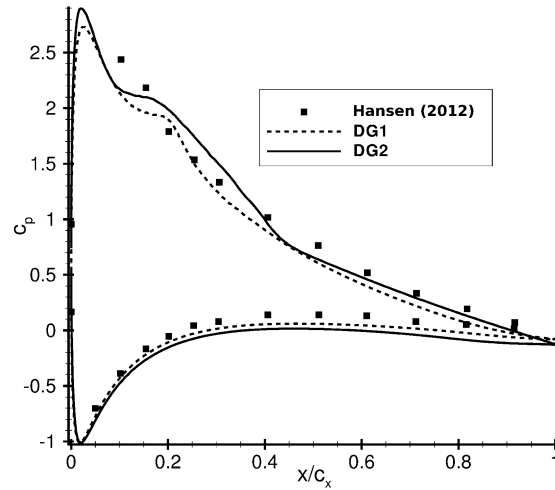


Fig. 6 Wall pressure coefficient distribution for NACA0012 at $\alpha_\infty=10^\circ$

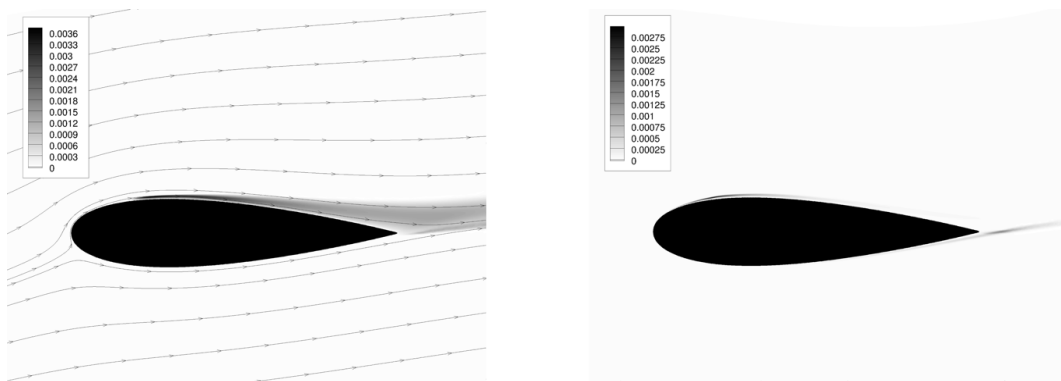


Fig. 7 NACA0021 at $\alpha_\infty=10^\circ$: dimensionless turbulent kinetic energy ($k/\mathcal{R}T_{in}^0$) with streamlines (left) and dimensionless laminar kinetic energy ($k_L/\mathcal{R}T_{in}^0$) (right)

Table 1 Lift and drag coefficients for NACA0021 at $\alpha_\infty=10^\circ$ and $Re_\infty=1.2 \cdot 10^5$

	C_l	C_d
Exp. from Hansen <i>et al.</i> (2011)	1.0	0.058
Present work LKE DG2	1.1	0.039

that the boundary layer on the suction side is characterised by separation and reattachment. The shear layer which defines the edge of the separation bubble is quite close to the airfoil and approximately aligned to the wall as can be verified by the computed results reported in Fig. 7. These conditions make it possible to properly describe the flow field by using a structured mesh with a strong clustering close to the wall. The mesh used in this work is a hybrid mesh defined by a structured region close to the wall surrounded by an unstructured region. It contains 17502 elements.

The computations were performed with both second (DG1) and third order (DG2) accurate DG schemes by using parabolic and cubic curvilinear wall elements, respectively. This allowed to

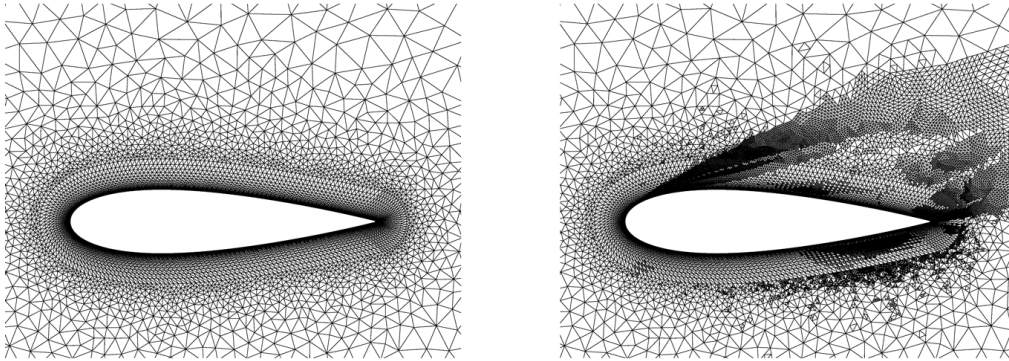


Fig. 8 Original (left) and adapted (right) unstructured meshes for the NACA0021 airfoil at $\alpha_\infty=16^\circ$

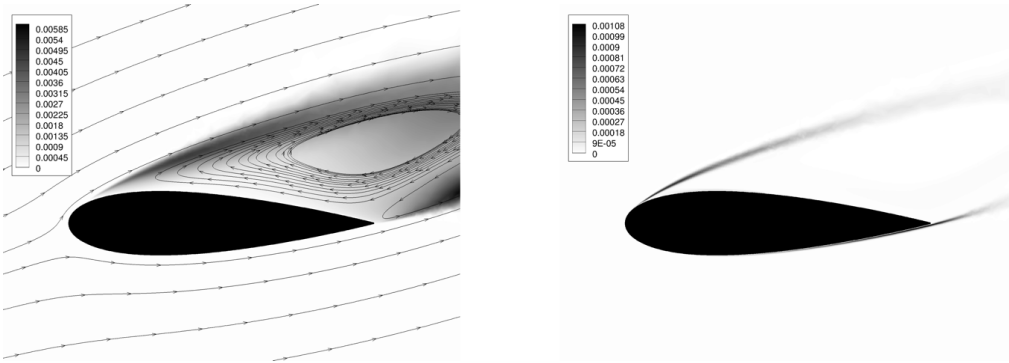


Fig. 9 NACA0021 at $\alpha_\infty=16^\circ$: dimensionless turbulent kinetic energy ($k/\mathcal{R}T_{in}^0$) with streamlines (left) and dimensionless laminar kinetic energy ($k_L/\mathcal{R}T_{in}^0$) (right)

Table 2 Lift and drag coefficients for NACA0021 at $\alpha_\infty=16^\circ$ and $Re_\infty=1.2 \cdot 10^5$

	C_l	C_d
Exp. from Hansen <i>et al.</i> (2011)	0.45	0.25
$\gamma-Re_{\theta t}$ from Choudhry (2015)	0.76	0.15
$k-\omega-k_L$ from Choudhry (2015)	0.75	0.21
Present work LKE mesh-0	0.28	0.17
Present work LKE mesh-1	0.26	0.17
Present work LKE mesh-2	0.25	0.17

perform a convergence study by showing how the numerical solution is affected by the increase in the number of degrees of freedom (52506 degrees of freedom per equation for DG1 and 105012 degrees of freedom per equation for DG2).

In Fig. 6 the computed wall pressure coefficient is reported for second and third order computations and compared to the experimental results from Hansen (2012). In Table 1 the computed lift and drag coefficients obtained by the third order scheme are compared to the experimental values. The results show reasonable agreement with the experimental data.

In Fig. 7 the turbulent kinetic energy and some streamlines obtained by the DG2 scheme are reported showing how the flow reattaches on the suction side after the separation bubble. The

Figure shows also the laminar kinetic energy field which allows to identify the small recirculation bubble on the suction side.

7.2 Post-stall working condition: $\alpha_\infty=16^\circ$

The flow field was studied also for a working condition defined by an angle of attack $\alpha_\infty=16^\circ$ and a Reynolds number $Re_\infty=1.2\cdot 10^5$. This working condition is characterized by a stall with a large recirculation region.

Since the shear layer is far from the body and its position is not known a priori, it is not trivial to generate a mesh with enough resolution in both the attached boundary layer and the separated shear layer. In order to solve this problem, the proposed adaptive algorithm is used. An initial coarse unstructured grid (Fig. 8 on the left) with 13624 triangles is used to start the simulation with the DG1 scheme. A stretching law is employed in the region close to the wall but, despite of this, the boundary layer is strongly under-resolved.

The approximate solution obtained on this original mesh is then automatically improved by the adaptive algorithm, which is called recursively two times. As can be seen in the final mesh (Fig. 8 on the right), the algorithm refines the grid in the boundary layer, in the recirculation region, in the shear layers and in the wake. The final results are reported in Fig. 9. In particular, the Figure shows the turbulent kinetic energy field and some streamlines in order to identify the recirculation region. The same Figure shows also the computed laminar kinetic energy field.

In Table 2, the lift and drag coefficients (C_l and C_d) obtained in the present work are reported for the initial and refined meshes.

They are compared with the experimental data obtained by Hansen *et al.* (2011) and reported by Choudhry *et al.* (2015). Furthermore, the numerical results obtained by Choudhry *et al.* (2015) with the $SST+\gamma-Re_{\theta t}$ model and the $k-\omega-k_L$ model of Walters and Cokljat (2008) are reported. The lift and drag coefficients obtained by the proposed approach converge as the algorithm automatically refines the mesh, as can be seen in Table 2. While the results for the other two transition models reported by Choudhry *et al.* (2015) overpredict the lift coefficient, the present results underpredict it. The drag coefficient obtained in the present study is in the range of the values predicted by the other two transition models. This comparison enlightens the difficulties related to the prediction of transitional flows by means of RANS equations. Indeed, all the considered models give very different lift coefficients which are far from the experimental value in this post-stall condition. As far as the LKE model is concerned, the definition of the vorticity thickness becomes inaccurate in some region of the considered flow, where the shear layer is far from being aligned to the wall. Furthermore, the use of a point vortex correction could have been useful to improve the prediction of the lift coefficient but it was not used in order to work with the same conditions adopted by Choudhry *et al.* (2015).

8. Conclusions

In this work the transitional flow on different airfoils is studied by means of a non-local laminar kinetic energy model. An algorithm for the evaluation of the non-local vorticity thickness is proposed and assessed on both hybrid and fully unstructured meshes. The algorithm is based on the definition of test lines which are independent from the grid lines. This helps in reducing the grid dependency effects related to the non-local term. The possibility to integrate the chosen

transition model on fully unstructured meshes can be exploited to perform detailed simulations in the presence of complex geometries, thanks to the flexibility of the unstructured approach.

Furthermore, a correction for removing possible unphysical values in the vorticity thickness field is introduced. This simple remedy makes the time integration of the governing equations significantly easier by avoiding some problems related to the stiff source terms of the model.

Since transition can take place in the separated shear layer far from the wall the classical y^+ check is not enough to guarantee a sufficient mesh resolution. For this reason, the use of an automatic adaptive algorithm is suggested for the considered flows. The proposed algorithm could be improved by the use of anisotropic splitting (see for example Leicht and Hartmann 2010) to distribute more efficiently the degrees of freedom in the boundary layer region.

As far as external flows are concerned, some sustaining terms are introduced in the original turbulence model in order to avoid the turbulence decay in the far field. These additional terms make the use of adaptive algorithms easier because they allow to get the chosen turbulence level at the leading edge even when coarse meshes are employed, as it is usually done at the beginning of an adaptive procedure. The use of the sustaining terms does not alter the transition process for the considered flows since the laminar kinetic energy generated in the shear layer and the related coupling term in the turbulent kinetic energy equation are significantly larger than the far field turbulent kinetic energy.

All the results presented in this work refer to 2D steady simulations. The employed implicit time integration scheme allows to get a steady solution by using a very large time step which can remove any unsteady structure in the separation region and in the wake. It would be possible to use a smaller time step to get an Unsteady-RANS simulation. This approach would show the evolution of the largest vortex structures but it would require the use of a 3D description because the physical evolution of the vortex structures at the considered Reynolds number is three-dimensional.

The proposed test line algorithm can be directly extended to 3D problems. Further investigations are required to define the best approach to follow when several solid walls are involved in 3D problems, for example close to the hub of a rotor blade. In this case the proposed algorithm would compute the vorticity thickness for each element by considering the solid wall closer to that element. This could introduce a discontinuity in the vorticity thickness field across the surface of the points which have the same distance from both the solid walls. A possible remedy could be adopted by introducing some corrections similar to those proposed in Section 5.3.

Further work should also be devoted to the definition of the boundary layer edge. In the present work the boundary layer edge is identified by performing a check on the total pressure in the direction normal to the wall. However, this approach cannot be used in the presence of a non-uniform total pressure distribution at the inlet and so alternative techniques should be introduced.

The obtained results show that the test line method gives reasonable results for flows with relatively moderate separation as in the T106c test case or the pre-stall case for the NACA0021. In particular, the obtained results for the T106c test case show good agreement with the experimental data if compared to other RANS studies (Babajee 2013) and to much more expensive 3D Large Eddy Simulations (De Wiart *et al.* 2012, De Wiart and Hillewaert 2015). Furthermore, the transition model used in this work introduces only one additional transport equation to the original RANS model while several common transition models (for example the $\gamma - Re_{\theta t}$ model) require two additional transport equations.

However, when the separation becomes too strong then the shear layer is far from being parallel to the solid wall and so the definition of vorticity thickness which is used in the LKE model

becomes inaccurate. Under these conditions, also the test lines approach and the corrections proposed in this work cannot recover an accurate approximation of the shear layer thickness and this could be the cause of the large differences between the computed results and the experimental data in the post-stall NACA0021 test case. However, the error with respect to the experimental value appears to be in the range spanned by other widely used transition models, as shown in Table 2.

In conclusion, the proposed approach could be useful to study the main features of the flow when moderate separations are considered and when the shear layer is not so far from being parallel to the solid wall in the transition region. Further investigations are required to extend the vorticity thickness definition to flows with large separations in which the evaluation of the thickness of the shear layer cannot be based on the wall normal direction. For this kind of flows, 3D Large Eddy Simulations represent a more reliable alternative if the associated huge computational cost can be afforded.

References

- Babajee, J. (2013), "Detailed numerical characterization of the separation-induced transition, including bursting, in a low-pressure turbine environment", Ph.D. Dissertation, Ecole Centrale de Lyon, Institut Von Karman de Dynamique des Fluides, Rhode-Saint-Genese, Belgium.
- Bassi, F., Botti, L., Colombo, A., Crivellini, A., Franchina, N., Ghidoni, A. and Rebay, S. (2010), *Very High-Order Accurate Discontinuous Galerkin Computation of Transonic Turbulent Flows on Aeronautical Configurations*, ADIGMA-A European Initiative on the Development of Adaptive Higher-Order Variational Methods for Aerospace Applications, 25-38.
- Bassi, F., Botti, L., Colombo, A., Di Pietro, D.A. and Tesini, P. (2012), "On the flexibility of agglomeration based physical space discontinuous Galerkin discretizations", *J. Comput. Phys.*, **231**(1), 45-65.
- Bassi, F., Crivellini, A., Rebay, S. and Savini, M. (2005), "Discontinuous Galerkin solution of the reynolds-averaged navier-stokes and $k-\omega$ turbulence model equations", *Comput. Flu.*, **34**(4), 507-540.
- Bode, C., Aufderheide, T., Friedrichs, J. and Kozulovic, D. (2014), "Correlation based inlet boundary conditions for improved turbulence and transition prediction in turbomachinery flows", *Proceedings of the 6th European Conference on Computational Fluid Dynamics*, Barcelona, Spain, July.
- Choudhry, A., Arjomandi, M. and Kelso, R. (2015), "A study of long separation bubble on thick airfoils and its consequent effects", *J. Heat Flu. Fl.*, **52**, 84-96.
- De Wiart, C.C. and Hillewaert, K. (2015), "A discontinuous Galerkin method for implicit LES of moderate Reynolds number flows", *Proceedings of the AIAA Aerospace Sciences Meeting, AIAA Science and Technology Forum*, Kissimmee, Florida, U.S.A., January.
- De Wiart, C.C., Hillewaert, K. and Geuzaine, P. (2012), "DNS of a low pressure turbine blade computed with the discontinuous Galerkin method", *Proceedings of the ASME Turbo Expo 2012 Turbine Technical Conference and Exposition*, Copenhagen, Denmark, June.
- Deters, R.W., Ananda, G.K. and Selig, M.S. (2014), "Reynolds number effects on the performance of small-scale propellers", *Proceedings of the 32nd AIAA Applied Aerodynamics Conference*, Atlanta, U.S.A., June.
- Ferrero, A., Larocca, F. and Puppo, G. (2015), "A robust and adaptive recovery-based discontinuous Galerkin method for the numerical solution of convection-diffusion equations", *J. Numer. Meth. Fl.*, **77**(2), 63-91.
- Geuzaine, C. and Remacle, J.F. (2009), "Gmsh: A 3-D finite element mesh generator with built-in pre-and post-processing facilities", *J. Numer. Meth. Eng.*, **79**(11), 1309-1331.
- Hansen, K.L. (2012), "Effect of leading edge tubercles on airfoil performance", Ph.D. Dissertation, The University of Adelaide, Adelaide, Australia.

- Hansen, K.L., Kelso, R.M. and Dally, B.B. (2011), "Performance variations of leading-edge tubercles for distinct airfoil profiles", *AIAA J.*, **49**(1), 185-194.
- Hourmouziadis, J. (1989), *Aerodynamic Design of Low Pressure Turbines*, AGARD, Blading Design for Axial Turbomachines, 40.
- Kozulovic, D. and Lapworth, B.L. (2007), "An approach for inclusion of a non-local transition model in a parallel unstructured CFD code", *Proceedings of the 5th SME/JSME Joint Fluids Engineering Conference*, San Diego, California, U.S.A., July.
- Langtry, R.B. and Menter, F.R. (2009), "Correlation-based transition modeling for unstructured parallelized computational fluid dynamics codes", *AIAA J.*, **47**(12), 2894-2906.
- Lardeau, S., Leschziner, M.A. and Li, N. (2004), "Modelling bypass transition with low-reynolds-number nonlinear eddy-viscosity closure", *Flow Turbul. Combust.*, **73**(1), 49-76.
- Leicht, T. and Hartmann, R. (2010), "Error estimation and anisotropic mesh refinement for 3d laminar aerodynamic flow simulations", *J. Comput. Phys.*, **229**(19), 7344-7360.
- Lukarski, D. and Trost, N. (2014), Paralution Project, <http://www.paralution.com>.
- Marciniak, V. (2015), "Modeling flows in low-pressure turbine cascades at very low reynolds numbers", *CEAS Aeronaut. J.*, **6**(2), 257-270.
- Marciniak, V., Weber, A. and Kugeler, E. (2014), "Modelling transition for the design of modern axial turbomachines", *Proceedings of the 11th World Congress on Computational Mechanics*, Barcelona, Spain, July.
- Mayle, R.E. and Schulz, A. (1997), "The path to predicting bypass transition", *J. Turbomach.*, **119**(3), 405-411.
- Michalek, J., Monaldi, M. and Arts, T. (2012), "Aerodynamic performance of a very high lift low pressure turbine airfoil (T106C) at low reynolds and high mach number with effect of free stream turbulence intensity", *J. Turbomach.*, **134**(6), 061009.
- Michelassi, V., Wissink, J. and Rodi, W. (2002), "Analysis of DNS and LES of flow in a low pressure turbine cascade with incoming wakes and comparison with experiments", *Fl. Turbul. Combust.*, **69**(3-4), 295-329.
- Osher, S. and Solomon, F. (1982), "Upwind difference schemes for hyperbolic systems of conservation laws", *Math. Comput.*, **38**(158), 339-374.
- Pacciani, R., Marconcini, M., Fadai-Ghotbi, A., Lardeau, S. and Leschziner, M.A. (2011), "Calculation of high-lift cascades in low pressure turbine conditions using a three-equation model", *J. Turbomach.*, **133**(3), 031016.
- Pandolfi, M. (1984), "A contribution to the numerical prediction of unsteady flows", *AIAA J.*, **22**(5), 602-610.
- Sjolander, R.L.S. and Langtry, R. (2002), "Prediction of transition for attached and separated shear layers in turbomachinery", *Proceedings of the 38th AIAA/ASME/SAE/ASEE Joint Propulsion Conference and Exhibit*, Indianapolis, Indiana, U.S.A., July.
- Spalart, P.R. and Rumsey, C.L. (2007), "Effective inflow conditions for turbulence models in aerodynamic calculations", *AIAA J.*, **45**(10), 2544-2553.
- Tucker, P.G. (2013), "Trends in turbomachinery turbulence treatments", *Prog. Aerosp. Sci.*, **63**(1), 1-32.
- Walters, D.K. and Cokljat, D. (2008), "A three-equation eddy-viscosity model for reynolds-averaged navier-stokes simulations of transitional flow", *J. Flu. Eng.*, **130**(12), 1-14.
- Walters, D.K. and Leylek, J.H. (2005), "Computational fluid dynamics study of wake-induced transition on a compressor-like flat plate", *J. Turbomach.*, **127**(1), 52-63.
- Wilcox, D.C. (1998), *Turbulence Modeling For CFD*, DCW Industries, La Canada, California, U.S.A.
- Yershov, S., Derevyanko, A., Yakovlev, V. and Gryzun, M. (2016), "Influence of laminar-turbulent transition on 3D flow pattern in subsonic turbine cascade", *Proceedings of the 52nd AIAA/SAE/ASEE Joint Propulsion Conference*, Salt Lake City, Utah, U.S.A., July.